Advances in Colloid and Interface Science, 39 (1992) 77–101
Elsevier Science Publishers B.V., Amsterdam

DYNAMICS OF CONTACT LINES IN FOAM FILMS

I.B.IVANOV, P.A.KRALCHEVSKY, A.S.DIMITROV AND A.D.NIKOLOV
Laboratory of Thermodynamics and Physico-Chemical Hydrodynamics, University of Sofia, Faculty of Chemistry, Sofia 1126, Bulgaria

ABSTRACT

Different factors can contribute to the value of the line tension acting at the periphery of a thin foam film. To study one of them, the motion of the contact line, a new experimental technique has been developed. It was established experimentally that slowly shrinking small air bubbles attached to a liquid - air interface form a nonequilibrium (dynamic) contact angles. Aqueous solution of sodium dodecyl sulfate (SDS) are used at two different concentrations of added electrolyte. A black thin liquid film is formed at the top of the bubble. The experimental cell used allows measurements with shrinking, expanding and quiescent ("stopped") bubbles. Hysteresis of the contact angle has been observed. The results show that the shrinking of the contact line (advancing meniscus) causes deviation of the contact angle from its equilibrium value. The data allow independent calculation of the film and line tensions, γ and κ. For a "stopped" bubble both γ and κ relax with time: κ tends to zero and γ tends to its equilibrium value for infinite film known from other experiments. The results suggest that the concept of *dynamic* line tension must be introduced. The latter was attributed to the motion of the contact line.

1. INTRODUCTION

The interest toward the line tension and its effect on the contact angles has been markedly increased during the last decade. The study of these effects is stimulated by their possible importance for the occurrence of a number of phenomena like wetting, flotation, interactions of fluid particles, biological cells, etc. Nevertheless, the information about the values of the line tension, obtained with different systems is still scanty and sometimes controversial. As a rule, the theoretical works predict systematically lower magnitude of the line tension than the magnitude determined experimentally. For attached emulsion droplets the theory [1,2] predicts line tension κ = 0.1nN, whereas the experiment [3] yields κ = 10 - 20nN. The theoretical values of κ for a solid-liquid-gas three phase contact line are between -0.026 and -0.082 nN [4]. On the other hand, for the same type of systems

0001-8686/92/$15.00

positive line tension of the order of 1000 nN has been measured experimentally [5,6]. Line tension of about -0.001nN has been estimated theoretically for the periphery of a thin foam film [7]. The measurements with thin films formed at the top of small floating bubbles yielded κ of the order of -100nN [8].

We think that these differences should not be considered as failure either of the theory or of the experiment. The theories of line tension are usually based on some simplified model concepts, whereas the real situation studied experimentally can be much more complicated. Different unexpected effects can contribute to the line tension.

We believe the difficulties with the line tension can be overcome by carrying out detailed studies of this effect with some simple systems. Such systems, investigated in the present study, are the foam films. In this case effects like surface roughness and inhomogeneity (typical for solid surfaces) are absent. In addition, the interactions in the thin film and the viscous effects accompanying its drainage are quite well understood (see e.g. [9]).

In the next section we give a brief outline of the theory of line tension at the periphery of the thin films. Special attention is paid to those effects, which can perturb the microscopic transition zone film-meniscus thus leading macroscopically to the appearance of an effective line tension. The remaining part of this paper is devoted to new experiments with small bubbles, in which the role of the contact line motion on the values of the contact angle and line tension is studied. We believe that these new experimental results explain the existing gap between theory and experiment.

2.MACROSCOPIC AND MICROSCOPIC TREATMENTS OF THE CONTACT ZONE FILM - MENISCUS

a) *Macroscopic treatment*

The force balance equations at the periphery of a thin liquid

film, as well as the related problem about the definition of the contact angle, are based on the Gibbs macroscopic theory of capillarity [10]. The latter was extended by Boruvka and Neumann [11] to linear and point phases.

For clarity we give a brief outline of the Gibbs approach. A detailed and rigorous treatment can be found in Refs. [10-14]. The transition regions between the phases in real non-homogeneous systems have finite thickness or width and the forces acting in them (more precisely, the pressure tensor) are continuous functions of the position. In the Gibbs treatment the phases are considered as being homogeneous, the transition regions are replaced by sharp boundaries (surfaces, lines or points) and the integrals over the pressure tensor are replaced by forces acting on the surfaces (e.g. surface tension) the lines and the points. In order to make these idealized (model) systems equivalent to the real ones, excesses of the extensive properties are also introduced. The positions of the phase boundaries (surfaces, lines and points) in the model systems are fixed by the conditions for equivalence of the real and model systems both mechanically and with respect to the extensive properties. In some cases the positions of a few boundaries can be chosen arbitrarily. Some of the macroscopic parameters so defined can depend on the localization of the boundaries (e.g. the surface tension of a drop depends on the drop radius [10,12,13]), i.e. on the choice of the idealized system, but once this choice has been made all parameters have well defined fixed values for a given physical state of the real system. For the line tension this problem was investigated by Navascues and Tarazona [15].

Two equivalent approaches have been used in the macroscopic theory of thin films: we call them the "membrane approach" when the film is considered as a membrane of zero thickness and one film tension γ acting along the surface of tension, and the "detailed approach" when the film is treated as a homogeneous liquid layer of thickness h and two film surface tensions, σ_1^f and σ_2^f (see Refs.

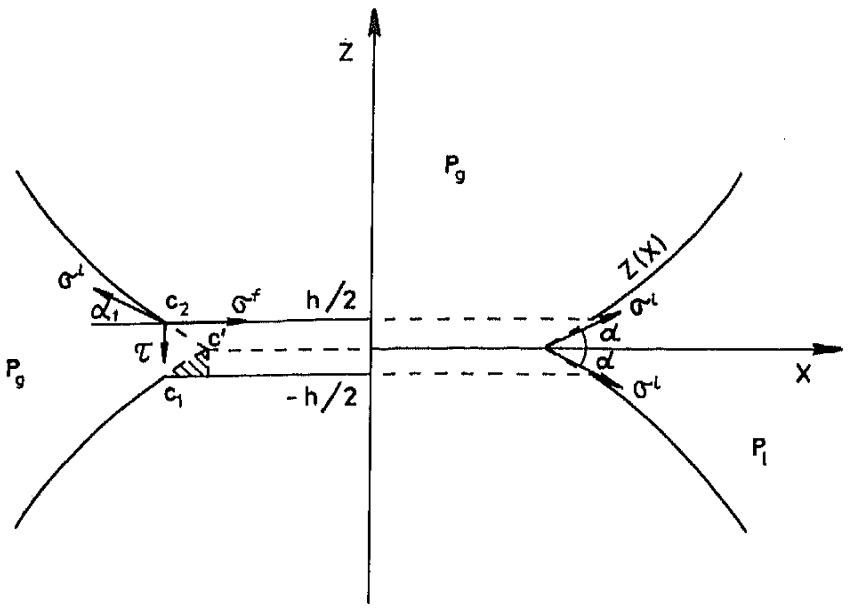

Fig.1. The membrane and the detailed approaches (on the right- and left-hand side, respectively).

[13,16]). All phase boundaries are assumed to be the surfaces or lines of tension (see Refs. [12,16,17]).

Let us consider a flat symmetrical thin liquid film ($\sigma_1^f = \sigma_2^f \equiv \sigma^f$) surrounded by a meniscus (with surface tension σ^l) in the absence of gravity - see Fig.1. Such films may have translational [18] or cylindrical [19] symmetry. The right-hand side of Fig.1 illustrates the membrane approach. The extrapolated meniscus surfaces z(x) (extrapolated at constant surface tension σ^l and capillary pressure [17]), meet at the contact line (at $x = r_c$) and form an angle 2α. For translational symmetry the balance of the forces acting along the axis Ox at the contact line yields

$$\gamma = 2\sigma^l \cos\alpha \qquad (1)$$

The force balance at the contact line along the axis Oz in this (membrane) approach is automatically satisfied. When the film has a cylindrical symmetry (then z(x) is the generatrix of the meniscus surface), Eq.(1) must include a term accounting for the line tension κ of the contact line C [20]:

$$\gamma + \frac{\kappa}{r_c} = 2\sigma^l \cos\alpha \qquad (2)$$

It was shown in Ref. [17] that the contact line defined by the extrapolation procedure described above is a line of tension, so that (2) does not contain the term $\frac{\partial \kappa}{\partial r_c}$ accounting for the virtual displacement of the contact line.

There are two contact lines and two film surfaces in the detailed approach (see the left-hand side of Fig.1, where C_1 and C_2 are the points where the two contact lines pierce the plane of the drawing). For cylindrical symmetry the contact lines are circumferences with radii r_{c1}. In the case of a film of finite thickness the contact angle $\alpha_1 \neq \alpha$ - see Fig.1 and Ref.[21]. The tangential condition for equilibrium (along Ox) in the detailed approach for translational symmetry was formulated by de Feijter and Vrij [7] and derived by a variational procedure by Toshev and Ivanov [22]:

$$\sigma^f = \sigma^1 \cos\alpha_1 \tag{3}$$

For axially symmetric films one can write for each contact line (see [7]):

$$\sigma^f + \frac{\tilde{\kappa}}{r_{c1}} = \sigma^1 \cos\alpha_1 \tag{4}$$

where $\tilde{\kappa} = \kappa_1 = \kappa_2$ is the line tension of the respective contact line C_1 or C_2.

In the detailed approach the normal balance

$$\tau = \sigma^1 \sin\alpha_1 \tag{5}$$

is not trivial. Here τ is the transversal tension, introduced in Refs. [23,24]. Values of τ for foam films stabilized with sodium dodecyl sulfate are published in Ref. [25]. In fact, Eqs. (4) and (5) are two projections of the vectorial equation

$$\underline{\sigma}^f + \underline{\sigma}^1 + \underline{\sigma}^\kappa + \underline{\tau} = 0 \tag{6}$$

where the vector $\underline{\sigma}^\kappa$ of magnitude $|\underline{\sigma}^\kappa| = \frac{\tilde{\kappa}}{r_{c1}}$ is directed toward the center of curvature of the contact line.

Since the membrane and the detailed approaches (models) are mechanically equivalent, there are equations connecting γ with σ^f and κ with $\tilde{\kappa}$:

$$\gamma = 2\sigma^f + P_c h \tag{7}$$

$$\kappa = 2\tilde{\kappa} + 2P_c\Delta A - 2\sigma^l\Delta l + 2\sigma^f\Delta r_c \tag{8}$$

where $P_c = P_g - P_l$ is the capillary pressure, ΔA is the area of the dashed curvilinear triangle in Fig.1, Δl is the length of the arc C_1C', $\Delta r_c = r_{c1} - r_c$. Eqs. (7) and (8) have been first derived in Refs.[13] and [23], respectively.

It is interesting to note, that when the line tension effect $\frac{\tilde{\kappa}}{r_{c1}}$ is not zero, the contact angles are gravity dependent [26]. Besides, the transversal tension τ turns out to be more important than the buoyancy force for attachment of small particles to interfaces [25].

The macroscopic parameters so defined are amenable to experimental measurement. The connection between the measured thermodynamic macroscopic parameters (surface tension, disjoining pressure, film and line tensions, etc.) and the force distribution in the real non-homogeneous system can be established only via a microscopic theory, allowing the representation of the thermodynamic parameters as integrals over the pressure tensor or some other equivalent forces, defined locally. Such a microscopic theory is presented in [7,9,24,27]. A brief outline is given below.

b) *Microscopic treatment*

Let us consider again a symmetrical planar thin liquid film, in the absence of external fields, encircled by a capillary meniscus of the same liquid (Fig.2). Close to the axis of symmetry Oz the film has constant thickness h (defined as the distance between the two surfaces of tension each of them with film surface tension σ^f). Far from Oz (in the meniscus) the disjoining pressure

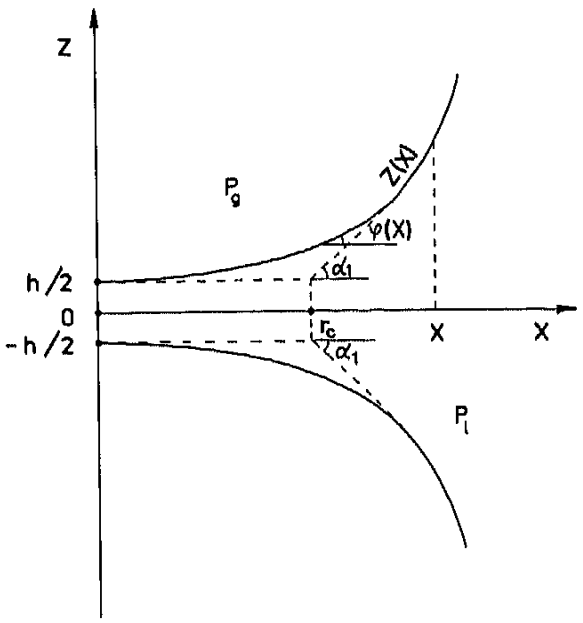

Fig.2. The transition between a thin liquid film and the capillary meniscus is smooth. The solid lines represent the real interfaces and the dashed - extrapolated ones.

$\Pi = 0$, the surface tension of the meniscus is constant, σ^1, and the generatrix of the surface $z(x)$ satisfies Laplace equation [28]. In the intermediate region the two surfaces interact and since the interaction energy depends on the distance between them, the surface tension in this region $\sigma(x)$ changes gradually from σ^f to σ^1. The disjoining pressure Π is also a function of x in this region. This (real) system is depicted in Fig.2 with continuous solid lines. As mentioned above it is customary to introduce an idealized system by extrapolating the meniscus and film surfaces (at constant surface tensions and capillary pressure [17]) until they intersect to form a contact angle α_1. The extrapolated surfaces are shown in Fig.2 with dashed lines.

We consider the film as divided by its surface of tension (in this case the surface z=0) into two parts and will define the local disjoining pressure as

$$\Pi(x) = P_N^0(x) - P_l \qquad (8)$$

where P_l is the pressure in the meniscus and $P_N^0(x)$ is the value of the component P_{zz} of the pressure tensor at the surface of tension.

Eq.(8) connects Π directly with statistical mechanics, because P_{zz} can be expressed through integrals over the intermolecular potentials and the pair correlation functions - see e.g. Ref.[12], Eqs.(34.6)-(34.8).

Let $\varphi(x)$ be the running slope angle of the meniscus surface:

$$\tan\varphi = \frac{dz}{dx} \tag{9}$$

By using the method of the local balance one can derive the tangential [7]

$$-\frac{d(\sigma\cos\varphi)}{dz} + \frac{\sigma\sin\varphi}{x} = P_c \tag{10}$$

and the normal [24]

$$\frac{d(\sigma\sin\varphi)}{dx} + \frac{\sigma\sin\varphi}{x} = P_c - \Pi(x) \tag{11}$$

capillary force balances at each point of a meniscus surface in the transition zone. Eqs.(9), (10) and (11) form a full set allowing the calculation of $z(x)$, $\varphi(x)$ and $\sigma(x)$ provided that $\Pi(x)$ is known from the molecular theory.

The elimination of P_c between Eqs.(10) and (11) yields [24]:

$$\frac{d\sigma}{dz} = -\Pi(x)\cos\varphi(x) \tag{12}$$

The latter equation, shows that hydrostatic equilibrium in the transition region is ensured by simultaneous variation of σ and Π.

Let x_B is large enough to ensure $\sigma(x_B) = \sigma^l$ - see Fig.2. Then by integrating Eqs.(10) and (11) as explained in Refs [9,24] one can derive

$$\kappa = 2r_c \int_0^{x_B} \left[\left(\frac{\sigma\sin^2\varphi}{x\cos\varphi}\right) - \left(\frac{\sigma\sin^2\varphi}{x\cos\varphi}\right)^{id}\right]dx \tag{13}$$

$$\tau = \frac{1}{r_c} \int_0^{x_B} \left[(\Pi)^{id} - \Pi(x)\right]x\,dx \tag{14}$$

where the subscript "id" refers to the idealized system, i.e. to the extrapolated meniscus surfaces. In particular

$$(\Pi)^{id} = P_c \quad \text{for } 0 < x < r_{c1} ;$$
$$= 0 \quad \text{for } x > r_{c1} .$$

One sees that τ is an integral effect due to the difference of the disjoining pressure in the real and idealized systems, whereas κ is also an integral effect but determined by $\sigma(x)$ and the slope angle $\varphi(x)$ rather then by $\Pi(x)$. The fact that κ and τ are represented as integrals over small differences suggests that they should be very sensitive to minor variations of the functions in the integrands. In this respect the replacement of $\sigma(x)$ in Eq.(10) by σ^1 may substantially affect the result of the calculations. We will come back to Eq.(13) by the end of this paper to discuss the experimental values for the line tension presented in the next section.

The substitution of τ from Eq.(14) into Eq.(5) yields

$$\sin\alpha_1 = \frac{1}{\sigma^1 r_{c1}} \int_0^{x_0} \left[(\Pi)^{id} - \Pi(x)\right] x dx \qquad (15)$$

Eq.(15) allows calculation of the equilibrium contact angle α_1 when the disjoining pressure distribution $\Pi(x)$ is known.

The microscopic theory of the transition region film–meniscus was generalized in Ref. [27] for nonequilibrium thin films of arbitrarily curved interfaces. Due to the more complicated geometry in this case the apparatus of the differential geometry was utilized. In particular, for the symmetrical film sketched in Fig.2, the following generalizations of Eqs.(10) and (11) were derived:

$$-\frac{d(\sigma\cos\varphi)}{dz} + \frac{\sigma\sin\varphi}{x} = P_c + \left[Q_{xx}^{in} - Q_{xx}^{out} - \left(Q_{xz}^{in} - Q_{xz}^{out}\right)\cot\varphi\right] \qquad (16)$$

and

$$\frac{d(\sigma\sin\varphi)}{dx} + \frac{\sigma\sin\varphi}{x} = P_c - \Pi(x) + \left[Q_{zz}^{in} - Q_{zz}^{out} - \left(Q_{xz}^{in} - Q_{xz}^{out}\right)\tan\varphi\right] \qquad (17)$$

Here Q_{xx}, Q_{zz} and Q_{xz} are the values of the respective components of the viscous stress tensor at the film surface, and the superscripts "in" and "out" indicate the fluids inside and outside the film. Eqs.(16) and (17) hold both for small Reynolds numbers. When the film surfaces are tangentially mobile (low surfactant concentrations), additional effects, like surface diffusion and surface viscosity, should be also taken into account - see Ref.[29].

Dynamic effects, due e.g. to viscosity and diffusion, can disturb the profile $\varphi(x)$ of the transition zone between the film and the meniscus as well as the distribution $\sigma(x)$ of the interfacial tension in this zone. In accordance with Eqs.(13) and (15) these effects can also contribute, along with the equilibrium interaction between the film surfaces, to the values of the line tension and the contact angle. Hence the concept of "dynamic line tension" can be introduced. In many respects it is analogous to the concepts of dynamic surface tension or dynamic contact angle. The new experimental data presented below demonstrate that the dynamic line tension can affect considerably the Neumann - Young force balance at the contact line encircling a foam thin film.

3. EXPERIMENTS WITH BUBBLES ATTACHED TO A LIQUID SURFACE

In our previous study [8] we investigated the contact angles formed with shrinking air bubbles attached to a liquid - air interface. The experiments yielded line tension values varying with the radius of the contact line and having a magnitude up to 100 nN for large bubbles. This line tension effect was accompanied with variations in the film tension, γ, of the black foam film formed at the top of the bubble. The careful check of the experimental procedure [30,31] confirmed the reliability of the obtained values of κ and γ. It should be noted that the equilibrium theory of de

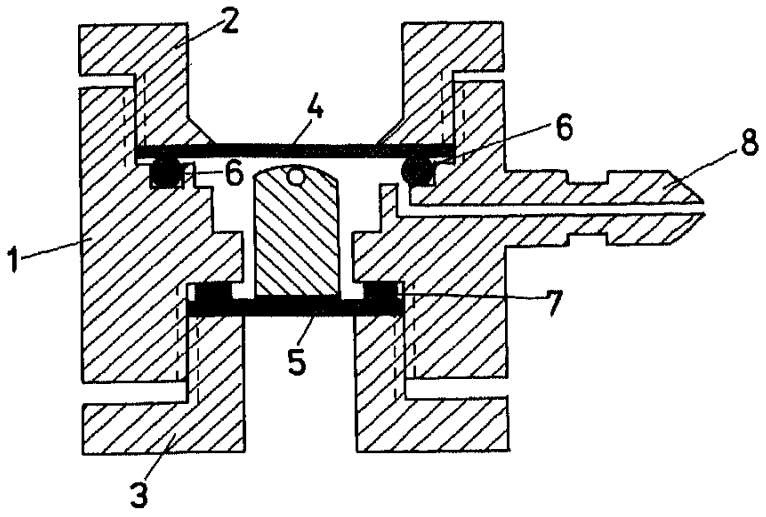

Fig.3. Experimental cell of variable pressure - cross section. 1 - teflon holder, 2 and 3 - screw covers, 4 and 5 - optical glass plates, 6 and 7 - isolation rings, 8 - connection with the pump.

Feijter and Vrij [7] predicts $\kappa \approx -0.001$ nN for Newton black films.

We believe that the only proper way to reveal the nature of the physical effects, giving rise to the large line tension values measured in [8], is to study directly the role of different factors on the contact angle, film and line tensions. The first thing we did was to check the role of the type of the surfactant. Toward this aim in [32] we replaced the anionic surfactant (SDS), used in [8] with a nonionic surfactant. The experimental results for this system yielded zero line tension.

The aim of the present study is to investigate the role of some nonequilibrium (dynamic) effects such as the motion of the contact line. An experimental cell of new construction allowed us to perform measurements with bubbles of diminishing, expanding and fixed constant equatorial radii.

A scheme of the new experimental cell is presented in Fig.3. The cylindrical holder 1, and the two screw covers, 2 and 3, are made from teflon. The upper and the bottom plates, 4 and 5 are optically plane-parallel glass. Two plastic rings, 6 and 7, placed between the glass plates and the holder, provide hermetic insulation of the cell interior from the outer air. The pressure

inside the cell can be controlled through the orifice 8, which is connected with the pump by means of teflon hoses. In our experiment we used a water jet pump.

A cylindrical glass vessel (of diameter 1.2cm and height 1.3cm) containing the surfactant solution is placed inside the cell. The solution forms a slightly convex meniscus, which keeps a small floating bubble at the center of the interface solution-air. At the beginning of each experiment the upper screw cover is open and a bubble of suitable size is blown out of a glass syringe. Then the cell is closed to allow saturation of the vapors above the solution. Before entering the cell, the air is pumped through a glass container partially filled with water. Thus saturation of the water vapors in the hoses is also ensured. The pressure adjustment is done by a special screw valve of fine pitch. In addition, a pet cock controls the connection of the system with the pump, or alternatively, with the atmosphere. In this way the pressure in the cell can be either decreased, or made equal to the atmospheric pressure.

In an hour and a half the bubble becomes small enough

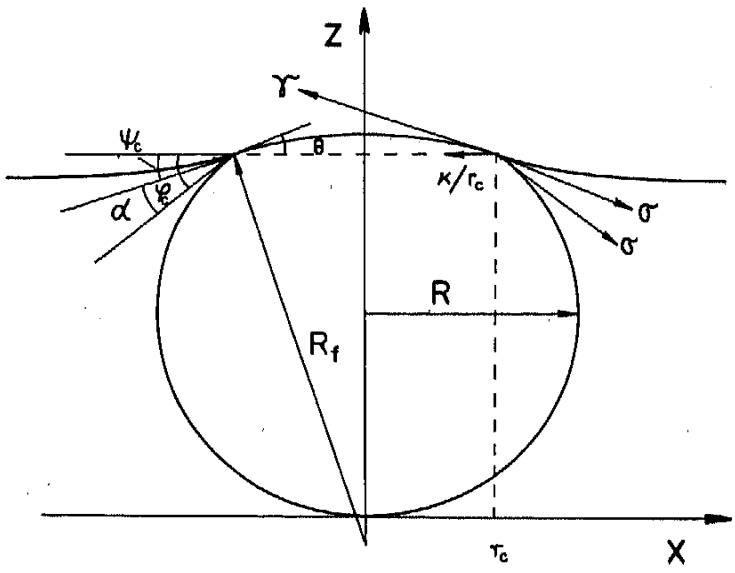

Fig.4. Cross section of an air bubble attached to a liquid - air interface. r_c, R and R_f are the radii of the contact line, bubble equator and film curvature, respactively; γ, σ and κ are the film, surface and line tensions.

(equatorial radius R < 300μm) and the measurements can be started. The radius r_c of the contact line (Fig.4) is measured in reflected light (illumination through the microscope objective). The equatorial bubble radius R is measured in transmitted light. To increase the accuracy, the values of r_c and R were recorded visually at the moment, when the diameter of the respective circumference was equal to an integer number of scale divisions. The measured values of R and r_c vs time t are interpolated by means of smooth curves as explained in Ref.[8]. The radius of curvature of the film R_f was measured by shearing differential interferometry by using method developed in Ref.[33].

The light source was a high - pressure mercury lamp (HBO - 50W) combined with a filter transmitting only the green spectral line of wavelength 546 nm. In order to produce interference pattern of better contrast we used illumination screen grid with a constant equal to 48μm, the same as in Ref. [33]. The principle of the differential interferometry and the construction of the microscope are described in detail in Refs. [34,35]. The application of the shearing method to measuring the curvature of fluid interfaces is given in Refs. [30,33,36].

A shearing distance d = 24μm was fixed at the beginning of each experiment and was not changed during the experiment. After the disappearance of the studied shrinking bubble, the radius of curvature, R_0, at the top of the convex liquid meniscus in the cylindrical container with the solution was measured. This was done by taking a photograph of the differential interference pattern created by this convex meniscus after removing the upper glass cover of the cell. A microscope objective (x6.3) was used in this case. The measured values of R_0 are necessary for calculating the shape of the meniscus around a bubble by using the procedure proposed in Ref.[31]

A typical photograph of the differential interference pattern

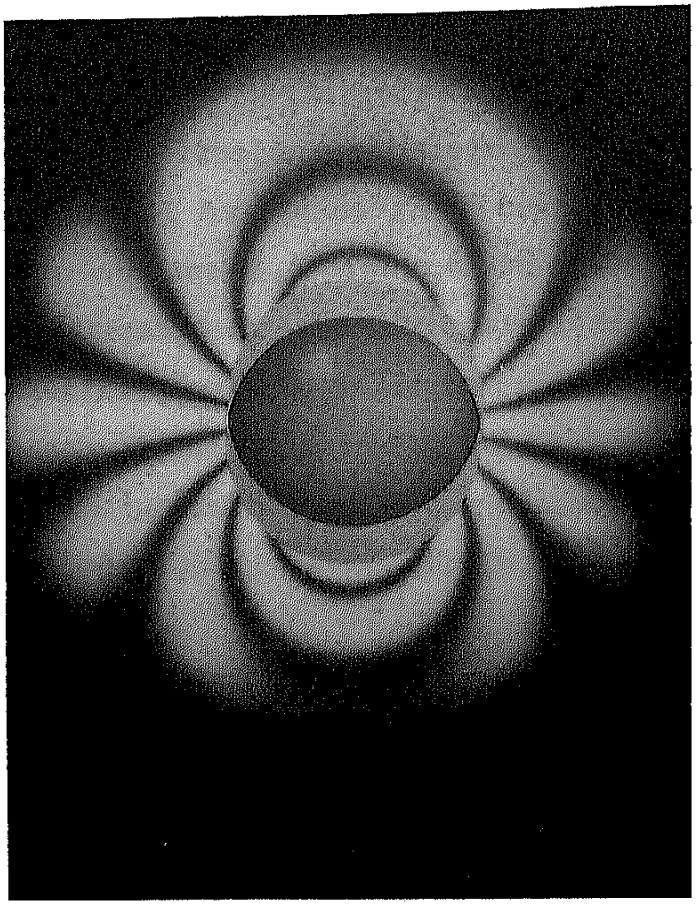

Fig.5. Differential interference pattern in light reflected from the cap of a floating bubble and the liquid meniscus around it.

created by the cap of the bubble (the film) is presented in Fig. 5. Just as in Refs. [32,33] three kinds of interference fringes, called "streaks", "rings" and "moustaches", are observed. In comparison with the experiments in Ref. [33] we used a longer - distance objective (x12.5) (instead of (x25)), because of the presence of the upper glass cover in the experimental cell of variable pressure. This led to the appearance of a greater number of streaks and rings than in Ref. [33].

As it is shown in Refs. [32,33] the streaks are due the light reflected by the spherical film, whereas the rings are due to interference of the light reflected by the film and the meniscus surfaces. One sees in Fig. 5 that the streaks appear on a darker background, than the rings. This is due to the higher reflectivity of the meniscus surfaces. As a result, it turns out, that the rings

yield the value of R_f with better accuracy at shorter exposure times than the streaks. That is why in the present work we used the rings for calculating R_f. In all cases when R_f was independently determined from streaks and rings on the same photograph, coincidence of the results was established in the framework of the experimental accuracy.

4. EXPERIMENTAL PROCEDURE AND RESULTS

The spontaneous diminishing of the bubble accelerates with time until eventually the bubble disappears. However the experimental cell in Fig.3 enables one to prevent the disappearance of the bubble and to investigate several subsequent spontaneous shrinkings of the same bubble. This is achieved in the following way.

When the equatorial bubble radius R comes down to about 150μm one suddenly decreases the pressure inside the cell (by using the water jet pump) and then one keeps it constant. In accordance with the ideal gas low $V=const/P_b$ volume V of a bubble, containing constant amount of gas, increases as the pressure P_b inside the bubble decreases. After a constant presure has been established the enlarged bubble starts again shrinking spontaneously and all measurements of r_c, R and R_f can be repeated. The values of the contact angle α (see Fig.4) are calculated from the measured R and r_c by using the procedure described in Section 3 of Ref.[8]. The only difference is that instead of the asymptotic formula (11) in [8] we used computer integration of Laplace equation in order to determine φ_c. This was neaded because the bubbles studied in the present work are larger than those in Ref.[8] and the asymptotic equations from Ref.[8] are less accurate than the numerical integration. The method for numerical integration of the Laplace

equation for the bubble surface is similar to the one used in Ref.[32].

Beside experiments with shrinking bubbles, the cell depicted in Fig.3 allows also studies of expanding bubbles. A bubble expands when the rate of shrinking due to the gas escaping from the bubble becomes smaller than the rate of expansion due to the decrease of the pressure inside the cell. The pressure decrease can be controlled by means of the screw valve. The procedure for measuring R and r_c, as well as the computation of the contact angle α, are the same as for shrinking bubbles. The rate of forced expansion in our experiments was 2 to 10 times higher than the rate of spontaneous shrinking.

The spontaneous diminishing of the bubble size can be stopped by a gradual decrease of the pressure inside the experimental cell, so that the effect compensates exactly the shrinking due to the gas escape. The process of spontaneous shrinking is relatively slow when the bubbles are not too small: its rate is $dR/dt \approx 0.025\mu m/s$ at $R = 200\mu m$ but it rises to $dR/dt \approx 0.40\mu m/s$ at $R = 80\mu m$. It

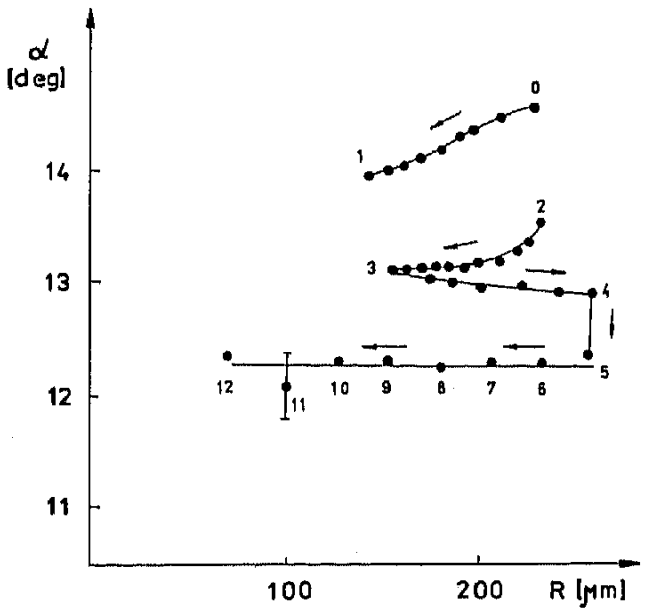

Fig.6. Values of the contact angle α of one and the same bubble at different conditions: 0-1 and 2-3 - spontaneous shrinkings; 3-4 gradual expansion, 4-5 relaxation at fixed R; 5,6,...,12 - equilibrium values of α for different fixed R.

turned out to be possible to keep R constant for large bubbles with an accuracy of ∓5μm by manual adjustment of the pressure (by means of the fine screw valve).

Curve 0-1 in Fig.6 represents the values of the contact angle α during the first spontaneous shrinking of a bubble formed in a 0.05% SDS solution with 0.25 mol/l NaCl. One sees that α decreases with R (i.e. with time). At the moment when R = 150 μm the bubble was forced to expand up to a radius R = 250 μm as described above. Tnis corresponds to transition from point 1 to point 2. Since the process is fast we could not measure values of R and r_c for this transition. Curve 2-3 shows the values of α during the second spontaneous shrinking of the same bubble. The contact angle is pronouncedly smaller compared with the first shrinking. When R came down to 150 μm (Point 3) the bubble was gradually expanded up to R = 260 μm (Point 4) with a mean velocity of the contact line dr_c/dt = 4 μm/min. Curve 3-4 shows that the contact angle α keeps the tendency (just like for the curves 0-1 and 2-3) to decrease with time although now R is increasing. When the radius reached R = 260μm the expanding was stopped and further decrease of α with time was observed - Curve 4-5. The contact angle relaxes for about 30 min and eventually attains some constant (equilibrium) value α_e (point 5).

After the relaxation 4-5, the bubble was allowed to shrink (by controlled increase the of pressure inside the cell) from R = 260μm to R = 230μm (from point 5 to point 6) and was stopped again. During this shrinking the contact anggle has a little icrease and then it relaxes again after R has been fixed. The equilibrium values, α_e, of α in points 5 and 6 turned out to coincide in the frames of the experimental accuracy. Then this procedure was repeated several times: all the transitions from 5-6 up to 11-12 correspond to shrinking, whereas the values of α in points 5, 6,...., 12 are the equilibrium contact angles reached after the relaxation. This experiment shows that the equilibrium value, α_e,

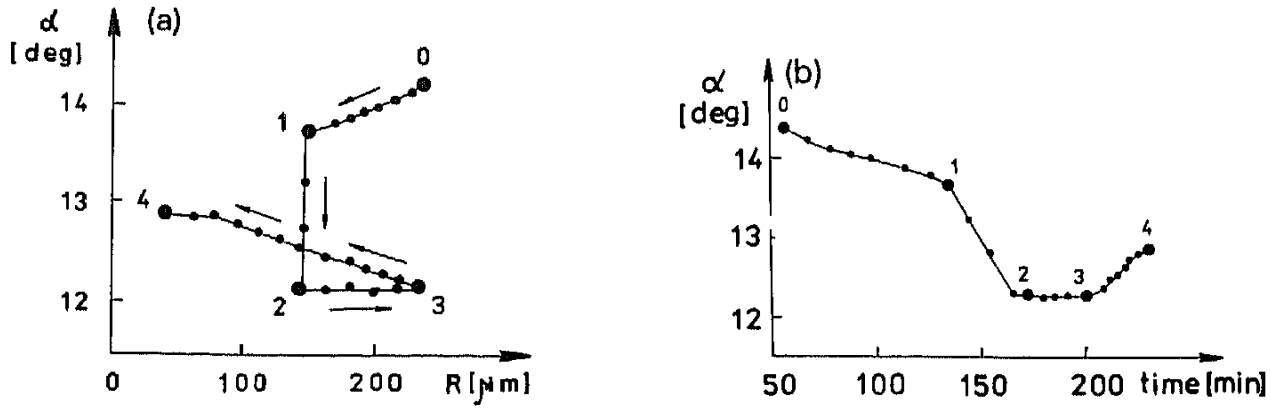

Fig.7. The contact angle α of an air bubble as a function of the equatorial bubble radius R (a), and of time (b). 0-1 - spontaneous shrinking; 1-2 relaxation at R = 152μm; 2-3 gradual expansion; 3-4 - spontaneous shrinking.

of the contact angle does not depend on the bubble size in the investigated range of radii.

Additional information about the dynamic behavior of the contact angle of small bubbles is provided by the experimental data about subsequent expansion and shrinking of a bubble that has reached previously equilibrium. This data are presented in Fig.7. In Fig.7a α is plotted versus the bubble radius R, whereas in Fig 7b the same data for α are represented as a function of time.

Curve 0-1 corresponds to the initial spontaneous shrinking of the bubble at atmospheric pressure. At R = 150μm the process of shrinking was stopped as described above. The contact angle of the stopped bubble with constant R decreased from 13.5^0 to an equilibrium value $\alpha = 12.2^0$. The relaxation (1-2) took 30 min. (If the bubble had not been stopped, it would have shrinked from R = 150μm to R = 0 for about 40 min.) Then the bubble was gradually expanded from R=150μm to R=220μm with an average rate dR/dt $\approx$ 2.5μm/min. It is important to emphasise that no changes of the contact angle were observed during this process of expansion: $\alpha = \alpha_e$ on the portion (2-3) of the curves in Fig.7. After the expansion, the bubble was allowed to shrink spontaneously again at constant pressure in the cell - curve (3-4). As shown in Fig.7, the

shrinking was accompanied by an increase of the contact angle. The latter exhibits a tendency of leveling off at a value of about 13^0 for the small bubbles (Fig.7a).

The comparison between the processes (2-3) and (3-4) in Fig.7 shows that in the case of a receding meniscus (expanding contact line) the contact angle maintains its equilibrium value, whereas in the case of an advancing meniscus (shrinking contact line) the contact angle increasingly deviates from its equilibrium value. Such behavior is typical for the hysteresis effects observed often with contact angles under dynamic conditions. In the case of smooth and homogeneous interfaces the hysteresis can be due to the interactions between the two meniscus surfaces [37].

The vertical and the horizontal projections of the Neumann - Young force balance provide two equations for independent calculation of the film tension, γ, and the line tension, κ (see Fig.4 and Eqs. [6-7] in Ref.[8]):

$$\gamma = \sigma\,(\sin\varphi_c + \sin\psi_c) \,/\, \sin\theta \qquad (18)$$

$$\kappa = \sigma r_c[\cos\varphi_c + \cos\psi_c - (\sin\varphi_c + \sin\psi_c)\,\cot\theta] \qquad (19)$$

Here σ is the solution surface tension,

$$\theta = \arcsin\left(\frac{r_c}{R_f}\right) \qquad (20)$$

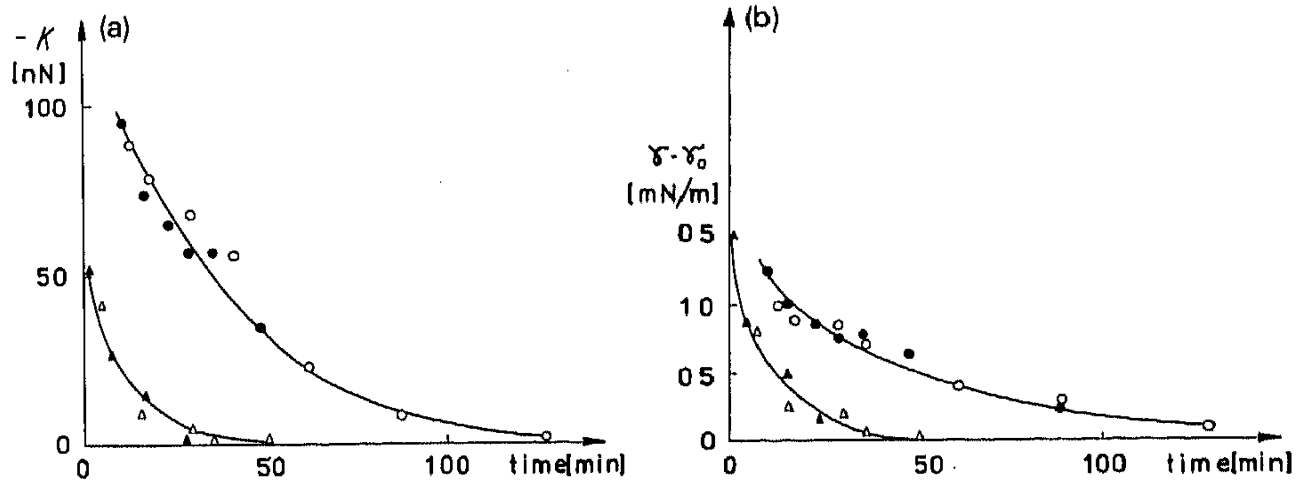

Fig.8. Relaxation of the line tension κ (a) and of the film tension γ (b) with time t at fixed equatorial bubble radius (0.25 mol/l NaCl).

and the angles φ_c and ψ_c are calculated as described in Refs.[8,32]. The dependence on the time t of the values of the line and film tensions, κ and γ respectively, calculated from Eqs.(18,19) for a stopped bubble (R = const; similar to the portions 4-5 and 1-2 in Figs. 6 and 7 respectively) are shown in Fig.8.

Time zero in Fig.8 corresponds to the time moment, when the equatorial radius R of an initially shrinking bubble was fixed by regulation of the pressure inside the experimental cell. γ_0 in Fig.8 is the equilibrium film tension of macroscopic films measured by de Feijter [18].

The values corresponding to the open and the full circles in Fig. 8 were measured with two stopped bubbles of radii R = 282μm and R = 265μm, respectively. The full and open triangles correspond to two smaller bubbles, both of them of radius R = 152μm. Each of these four bubbles was formed in a SDS solution containing 0.25 mol/l NaCl. Each point corresponds to the moment when a photograph of the differential interference pattern was taken. The data demonstrate that both the film tension, γ, and the line tension, κ, exhibit relaxation with time. κ tends to zero in the framework of the experimental accuracy. γ tends to its equilibrium value γ_0 = 64.4mN/m, measured by de Feijter [18] with macroscopic rectangular

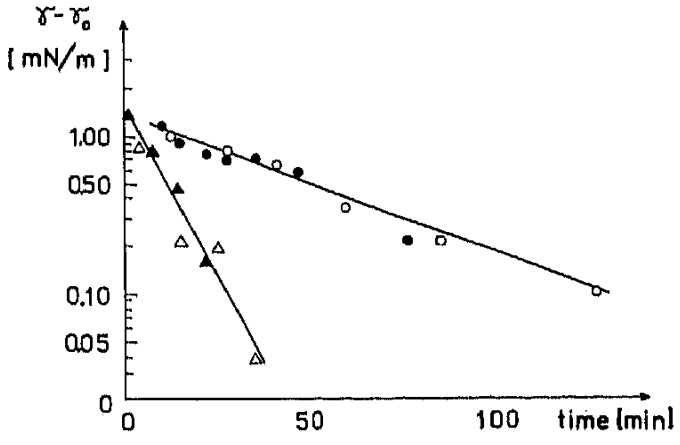

Fig.9. The data for the film tension γ from Fig. 8b presented in a log scale vs time t.

films. Obviously the smaller bubbles relax faster than the larger ones.

Fig. 9 represents the same data as in Fig. 8b, but on a log scale on the ordinate axis. The slope yields relaxation time $\tau_1 \approx$ 50min for the larger bubbles and $\tau_2 \approx$ 10min for the smaller ones. The respective contact radii (upon full relaxation) are $r_{c1} = 85\mu m$ and $r_{c2} = 37\mu m$. It is interesting to note that $\frac{\tau_2}{\tau_1} \approx \frac{r_{c2}^2}{r_{c1}^2} \approx 0.19$, i.e. the larger the film area, the longer the relaxation. The relaxation times calculated from the data for κ (Fig. 8a) coincide with τ_1 and τ_2 as determined from the relaxation of γ (Fig. 8b). Similar results were obtained with the solution of SDS containing 0.32 mol/l NaCl.

5. CONCLUSIONS

The general conclusion from the experiments described in the previous section is that the contact angle, film and line tensions of spontaneously shrinking bubbles in the investigated solutions have nonequilibrium values. This conclusion is based on the following facts.

There is pronounced difference between the contact angles measured during two consecutive spontaneous shrinkings realized with the same bubble - compare curves (0-1) and (2-3) in Fig.6.

When the spontaneous shrinking of a bubble is stopped by fixing the equatorial radius R (i.e. the capillary pressure) a relaxation of the contact angle α is observed - see curve (4-5) in Fig.6 and (1-2) in Fig.7. During the relaxation α changes with more than 1^0 for the investigated solutions.

If after the contact angle has relaxed the bubble is allowed to shrink spontaneously again, the contact angle deviates from its

equilibrium value, α_e, and starts increasing - see curve (3-4) in Fig.7. The latter fact implies that the shrinking of the contact line causes deviation of the contact angle from its equilibrium value.

The new experiments with small air bubbles described in this paper confirm the large values of the film and line tension ($\gamma > 2\sigma^1$, $\kappa \sim -100$nN) measured in Ref. [8] with shrinking bubbles formed in 0.05% aqueous solutions of sodium dodecyl sulfate at 0.25 and 0.32 mol/l added NaCl. (see the values of γ and κ in Fig.8 at the earlier times.)

Similarly to the contact angle α, the film and line tensions, γ and κ, of a "stopped" bubble exhibit relaxation. The relaxation time is longer for the larger bubbles (see Figs.8,9).

During the relaxation the parameters α, γ and κ are connected through the equation (cf. Eq. (1) in Ref. [38]).

$$\frac{1}{\cos\frac{\alpha}{2}} - \frac{2\sigma}{\gamma} + \frac{\kappa}{\gamma r_c} = 0 \qquad (21)$$

For example, the data in Fig. 8 (the larger bubble) shows that the change of the first term in Eq. (21) during the relaxation is 0.0023, of the second term: -0.0189, and of the third term: -0.0162. The conclusion is that the variations of the film and line tensions counterbalance each other in order the equilibrium condition, Eq. (21), to be satisfied.

The line tension κ during the relaxation tends to zero in the framework of the experimental accuracy ($\mp$15nN). This experimental finding is compatible with the theoretical result of de Feijter and Vrij [7], who calculated $\kappa = -0.001$nN for equilibrium Newton black films.

The film tension γ tends during the relaxation to an equilibrium value, which agrees well with the value measured by de Feijter [18] with macroscopic equilibrium films.

The results for γ are also in agreement with the experiments of Platikanov et al. [39], who recovered de Feijter's equilibrium

values of γ in experiments with bubbles fixed at the tip of a capillary (immobile contact line).

The new data shed some light on the line tension measurements with shrinking bubbles. In particular, the change of the contact angle with the bubble radius, which was interpreted in Ref. [40] as a line tension effect can well be due to the observed nonequilibrium phenomena. This arouses considerable doubt about the reliability of the line tension values reported in a number of publications [40-45].

The results from the present study suggest the introduction of a concept of a "dynamic line tension", analogous to the "dynamic interfacial tension" and "dynamic contact angle". It is worthwhile noting that the equilibrium line tension, as predicted by the theory [4,7], is an extremely small quantity (of the order of 10^{-11} - 10^{-12} N), so it usually turns out to be below the threshold of the experimental accuracy. On the other hand, the dynamic line tension can be many orders of magnitude greater. It can affect the value of the contact angle and the processes accompanying the motion of a three - phase contact line.

The processes giving rise to the dynamic line tension deserve a separate study. They are probably connected with local alterations of the interfacial shapes and tensions in a narrow vicinity of the three - phase contact zone. In accordance with Eqs.(13) and (15) such alterations contribute to the value of the line tension and contact angle.

We hope the results will be useful in all cases when the interaction between colloidal particles is accompanied with formation of a three - phase contact line: flotation of ores; stability of emulsions and microemulsions; interaction of a biological cell with other cells, with droplets or with solid surfaces, etc.

REFERENCES

1 V.M.Starov and N.V.Churaev,Kolloidn.,Zh.42 (1980) 703.
2 N.V.Churaev and V.M.Starov,J.Colloid Interface Sci.,103 (1985) 301.

3 J.A.Wallace and S.Schurch,J.Colloid Interface Sci.,124 (1988) 452.
4 P.Tarazona and G.Navascues,J.Chem.Phys.,75 (1981) 3114.
5 J.Gaydos and A.W.Neumann,J.Colloid Interface Sci.,120 (1987) 76.
6 D.Li and A.W.Neumann,Colloids Surfaces,43 (1990) 195.
7 J.A.de Feijter and A.Vrij,J.Electroanal.Chem.,37 (1972) 9.
8 P.A.Kralchevsky,A.D.Nikolov and I.B.Ivanov,J.Colloid Interface Sci.,112 (1986) 132.
9 I.B.Ivanov (Ed.),Thin Liquid Films,Dekker,New York,1988.
10 J.W.Gibbs,The Scientific Papers of J.Willard Gibbs,Vol.1. Thermodynamics, Dover, New York,1961.
11 L.Boruvka and A.W.Neumann,J.Chem.Phys.,66 (1977) 5464.
12 S.Ono and S.Kondo,Molecular Theory of Surface Tension in Liquids. Handbuch der Physik,Vol.10,Springer,Berlin,1960.
13 A.I.Rusanov,Phase Equilibria and Surface Phenomena, Khimia, Leningrad, 1967 (in Russian); Phasengleichgewichte und Grenzflachenerscheinungen, Akademie-Verlag,Berlin,1978.
14 A.I.Rusanov,in F.C.Goodrich and A.I.Rusanov (Eds.), The Modern Theory of Capillarity, Akademie-Verlag,Berlin,1981.
15 G.Navascues and P.Tarazona,Chem.Phys.Letters,82 (1981) 586.
16 P.A.Kralchevsky and I.B.Ivanov,in K.L.Mittal (Ed.),Surfactants in Solution, Plenum Press, New York, 1986, p. 1549.
17 I.B.Ivanov,B.V.Toshev and B.P.Radoev, in L.Padday (Ed.),Wetting, Spreading and Adhesion,Academic Press,London,1978,p.37.
18 J.A.de Feijter,Ph.D.Thesis.University of Utrecht,1973;
J.A.de Feijter and A.Vrij,J.Colloid Interface Sci.,64 (1978) 269
19 B.V.Derjaguin and A.S.Titievskaja,Kolloidn.Zn.,15 (1953) 416.
20 G.A.Martynov,I.B.Ivanov and B.V.Toshev,Kolloidn.Zn.,38 (1976) 474.
21 I.B.Ivanov and B.V.Toshev,Colloid Polymer Sci.,253 (1975) 593.
22 B.V.Toshev and I.B.Ivanov,Colloid Polymer Sci.,253 (1975) 558.
23 P.A.Kralchevsky and I.B.Ivanov,Chem.Phys.Lett.,121 (1985) 111.
24 P.A.Kralchevsky and I.B.Ivanov,Chem.Phys.Lett.,121 (1985) 116
25 A.D.Nikolov,P.A.Kralchevsky,I.B.Ivanov and A.S.Dimitrov, AIChE Simposium Series No.252,vol.82 (1986) 82.
26 I.B.Ivanov,P.A.Kralchevsky and A.D.Nikolov,J.Colloid Interface Sci.,112 (1986) 97.
27 P.A.Kralchevsky and I.B.Ivanov,J.Colloid Interface Sci.,137 (1990) 234.
28 H.M.Princen,in E.Matijevic and F.R.Eirich (Eds.),Surface and Colloid Science,Wiley,New York,1969,p.1.
29 I.B.Ivanov and D.S.Dimitrov,in I.B.Ivanov (Ed.),Thin Liquid Films, Dekker, New York,p.379.
30 A.D.Nikolov,A.S.Dimitrov and P.A.Kralchevsky,Optica Acta,33 (1986) 1359.
31 A.S.Dimitrov,A.D.Nikolov,P.A.Kralchevsky and I.B.Ivanov, J.Colloid Interface Sci. - submitted.
32 L.A.Lobo,A.D.Nikolov,A.S.Dimitrov,P.A.Kralchevsky and D.T.Wasan, Langmuir, 6 (1990) 995.
33 A.D.Nikolov,P.A.Kralchevsky and I.B.Ivanov,J.Colloid Interface Sci.,112 (1986) 122.
34 H.Beyer,Theorie und Praxis der Interferenzmikroskopie, Akademische Verlagsgeselschaft,Leipzig,1974.
35 H.Beyer,Jenaer Rundsch.,16 (1971) 82.
36 A.S.Dimitrov,P.A.Kralchevsky,A.D.Nikolov and D.T.Wasan, Colloids Surfaces, 47 (1990) 299.
37 G.A.Martynov,V.M.Starov and N.V.Churaev,Kolloidn.Zh.,39 (1977) 472.
38 I.B.Ivanov,A.S.Dimitrov,A.D.Nikolov,N.D.Denkov and P.A.Kralchevsky, J.Colloid Interface Sci.- accepted.

39 D.Platikanov,M.Nedyalkov and N.Rangelova, Colloid Polym.Sci., 265 (1987) 72.
40 D.Platikanov,M.Nedyalkov and V.Nasteva,J.Colloid Interface Sci., 75 (1980) 620.
41 B.V.Toshev,D.Platikanov and A.Scheludko,Langmuir,4 (1988) 489.
42 M.Nedyalkov and D.Platikanov,Abhanlungen Akad.,Wissensch. DDR, VI Intern. Tag. Grenzfl. Stoffe, Nr.1N,p.123, Akademie-Verlag,Berlin,1985
43 A.Scheludko,B.V.Toshev and D.Platikanov,in F.C.Goodrich and A.I.Rusanov (Eds.), The Modern Theory of Capillarity,Akademie- Verlag,Berlin,1981.
44 D.Platikanov and M.Nedyalkov,in J.M.Georges (Ed.), Microscopic Aspects of Adhesion and Lubrication,Elsevier,Amsterdam,1982,p.97.
45 A.Scheludko, Colloid Chemistry, Mir, Moscow, 1984, p.261-in Russian.